IIETA International Information and Engineering Technology Association
Advancing the World of Information and Engineering

Journal of New Materials for Electrochemical Systems
Vol.22, No.2, April, 2019, pp. 85-90
http://new-mat.org
http://iieta.org/journals/jnmes

Microstructure and hydration mechanism of autoclaved aerated concrete from fly ash

Zhaojia Wang[1], Jun Li[2,*], Pengfei Ye[2], Changlong Wang[2,3,4,†] and Xiaowei Cui[5]

[1] State Key Laboratory of Solid Waste Reuse for Building Materials, Beijing Building Materials Academy of Science Research, Beijing 100041,China
[2] School of Civil Engineering, Hebei University of Engineering, Handan Hebei Province, 056038, China
[3] Jiangxi Key Laboratory of Mining Engineering, Jiangxi University of Science and Technology, Ganzhou Jiangxi Province 341000, China
[4] Tianjin Sunenergy Sega Environmental Science & Technology Co. Ltd, Tianjin 300000, China
[5] Shaanxi Key Laboratory of Comprehensive Utilization of Tailings Resources, Shangluo University, Shangluo Shaanxi Province 726000, China

Corresponding Author Email: 9195922@qq.com; baistuwong@139.com

ABSTRACT

Autoclaved aerated concrete(AAC) with excellent mechanical properties were prepared by the grade II fly ash (FA) as siliceous materials, which was supported by the thermal power plant. The composition, morphology and thermal properties of the hydration products with different stages of AAC were detected by using X-Ray diffraction (XRD), scanning electron microscope (SEM), flourier transform-infrared spectroscopy (FT-IR), and thermogravimetric/differential scanning calorimeter (TG-DSC). Results shows that the main hydration products including ettringite (AFt), low crystallinity of C-S-H gels and $Ca(OH)_2$ were generated in the hardening body. After heat preservation 0 hour, the new hydration products tobermorite were detected. After heat preservation 8 houra, the major hydrated products were tobermorite and C-S-H gels in the final AAC samples. XRD diffraction peaks of the original mineral composition in FA were reduced, which indicated that the mineral composition of FA was decomposed, and the reaction between active components of SiO_2, Al_2O_3, and $Ca(OH)_2$ caused the formation of tobermorite under conditions of high temperature and pressure and hot alkaline activation.

Keywords: *fly ash; siliceous materials; autoclaved aerated concrete; ettringite; tobermorite*

Received: February-14-2019, Accepted: April-29-2019, https://doi.org/10.14447/jnmes.v22i2.a04

1. INTRODUCTION

Fly ash (FA) refers to the dust and furnace bottom slag collected from the flue gas of coal-fired (coal gangue, slime) boilers. China is one of the few countries in the world using the coal as its main energy source. In the past decade, with China's power industry developing rapidly, the total number of coal-fired generating units has continued to expand, and more than half of the coal resources in China have been consumed, resulting in the increase of FA year by year. According to statistics, in 2011 China's FA output reached 540 million tons. Moreover, as the country attaches greater importance to the comprehensive utilization of FA, the comprehensive utilization of FA is also increasing year by year. During the 13th Five-Year Plan period, China's comprehensive utilization rate of FA maintained a high level, even surpassing the United States and Japan. In 2018, its comprehensive utilization rate reached 68% [1].

At present, the FA has been used as prime materials in many building products such as the concrete admixtures, cement batching, aerated concrete blocks, FA brick, and FA ceramsite etc. [2-7]. Among them, autoclaved aerated concrete (AAC) is a new type of wall construction material, which has the advantages of light weight, good thermal insulation performance and strong processability. This technology for preparing aerated concrete using FA has been adopted for decades. A large amount of related research mostly focused on the effects of mix ratio, type and structure of hydration products on mechanical properties, carbonization properties, and drying shrinkage properties of AAC [8-13], but there have been few studies on the mechanism of the AAC during hydration. In view of the above, this paper attempts to explore the reaction mechanism of the AAC at different curing stages using the methods of X-ray diffraction (XRD), Fourier transform infrared spectroscopy (FT-IR), thermogravimetric-differential scanning calorimetry (TG-DSC), and scanning electron microscopy (SEM).

2. MATERIALS AND METHODS

2.1. Materials

(1) Fly ash. Class II low-calcium FA produced by a thermal power plant. Its chemical composition is shown in Table 1.

(2) Cement. The 42.5 ordinary Portland cement (OPC), with the

Table 1. Chemical composition of the raw materials (wt. %)

Materials	SiO_2	Al_2O_3	Fe_2O_3	MgO	CaO	Na_2O	SO_3	K_2O	Loss
FA	74.67	12.77	0.86	0.70	1.41	3.54	—	3.94	0.61
OPC	22.19	4.15	3.19	1.39	64.21	—	0.70	0.71	2.42
Lime	6.01	3.32	1.28	3.69	77.66	—	0.62	1.05	3.87
FGDG	3.16	1.35	0.49	7.49	33.38	0.13	45.70	0.18	8.28

fineness (≤0.08 mm) of 2.1%. Table 1 and 2 show its chemical composition and physical properties respectively.

(3) Lime. The main components are shown in Table 1; the lime used has a digestion time of 15 minutes, a digestion temperature of 65 °C, an effective CaO content of> 60%, and a 200-mesh sieve residue 12% to 15%;

(4) Flue gas desulfurization gypsum (FGDG). FGDG is from thermal power plants, the content of CaO and SO_3 is high, followed by SiO_2, MgO and Al_2O_3, and the fineness (⩾0.08 mm) is 16%. Its chemical composition analysis is shown in Table 1.

2.2. Sample preparation

Firstly, accurately weigh and mix the raw materials in a certain ratio, and then add warm water at 55 °C and stir for 2 minutes. Next, add a certain amount of aluminium powder into the slurry and stir for 1 minute. The stirred slurry was then quickly poured into 100 mm × 100 mm × 100 mm mould, and placed in a thermostatic curing box with a set temperature of 60 °C for 3-hour static curing. After the slurry in the mould was hardened and formed, the mould was removed and the hardened aerated concrete (HAC) was put in an autoclave for autoclaving and curing. During the autoclaving process, the pressure was controlled at about 1.2 MPa, the temperature was 185 °C, and the holding time was divided into two types: 0 hour (for AC-0 samples) and 8 hour (for AC-8 samples): the former is to stop heating the autoclave and naturally reduce the temperature of the autoclave to room temperature when the temperature and pressure in the autoclave reach the set values, while the latter is to continuously heat the autoclave when the internal temperature and pressure reach the set values, keep the autoclave at the set temperature and pressure for 8 hours, and then stop heating the autoclave.

2.3. Property characterization

The Rigaku D/Max-RC X-ray powder diffractometer (XRD) was used to analyse the mineral composition change of each sample, at the scanning speed of 4°/min, the scanning range of 5°~75°, the step size of 0.02°, and the Cu target. A NEXUS70 FT-IR spectrometer (test range 350~4000 cm^{-1}) was applied to qualitatively analyse the vibration of each functional group in the sample. A TG-DSC 204 integrated thermal analyser was adopted to perform thermogravimetric analysis on the samples, with the heating rate of 10 °C/min, the test temperature ranging from room temperature to 1000 °C, and air atmosphere. The SUPPA™ 55 field emission scanning electron microscope produced by Zeiss, Germany was used to carry out the morphology observation and energy spectrum analysis of the samples.

3. RESULTS AND DISCUSSION

3.1. XRD analysis of samples

Fig. 1 shows the XRD comparison charts of FA, HAC, AC-0 and AC-8 samples. It can be seen from the FA curve that the main mineral components of FA used in the test were quartz, plagioclase, anorthite and soda feldspar. On the HAC curve, XRD diffraction peaks of new

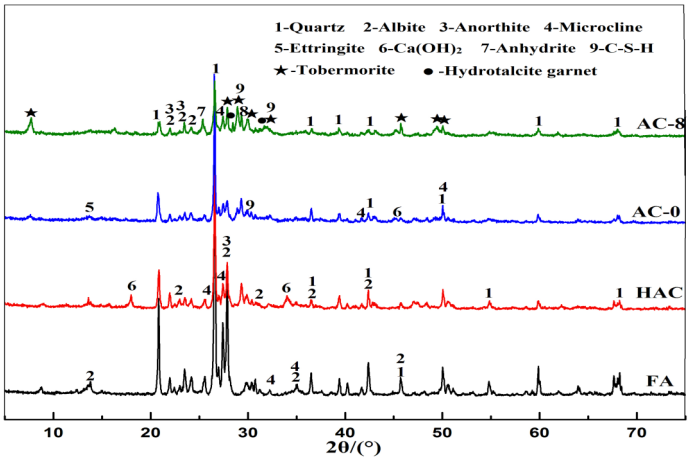

Figure 1. X-ray diffraction patterns of samples

phases such as ettringite (AFt), calcium silicate hydrate (C-S-H gels), $Ca(OH)_2$, and calcite appeared, and the XRD diffraction peaks of the main mineral components in the raw FA were reduced; among them, $Ca(OH)_2$ was produced by the cement-water hydration reaction and the lime-water digestion; calcite was formed by the carbonization reaction of hydration products (C-S-H gels) with CO_2 in the air; AFt was produced for two main reasons: first, in the presence of gypsum, calcium aluminate hydrate formed by cement hydration was combined with sulphate ions to generate the calcium sulphoaluminate hydrate crystals, namely AFt; Second, under alkaline conditions, a small amount of ultrafine particles in FA began to show chemical reactivity, and react with Ca $(OH)_2$ in the slurry to produce corresponding hydration products, such as C-S-H gels and calcium aluminate hydrate crystals, while the latter can quickly form AFt crystals in the presence of FGDG. These are also the reasons why the XRD diffraction peaks of the main mineral components for the FA were reduced in the HAC curve. Meanwhile, the formed AFt crystals and C-S-H gels were also the main sources of HAC strength.

Comparing the AC-0 and HAC curves, it can be found that the XRD diffraction peaks of AFt, C-S-H gels and Ca $(OH)_2$ in the AC-0 samples decreased, and those of the main mineral components in FA were also further reduced. Then, there appeared the XRD diffraction peaks of new tobermorite crystals, hydrated garnet and anhydrite. This is mainly because during the autoclave curing process, as the temperature and pressure increase, the dissolution rate of SiO_2 and Al_2O_3 in FA was accelerated, and more SiO_2 and Al_2O_3 components reacted with $Ca(OH)_2$ to form corresponding hydration products (such as C-S-H gels and calcium aluminate hydrate crystals); with the increase of SiO_2 dissolution, the Ca/Si in the liquid phase decreased, and the bi-alkaline C-S-H gels formed in the early stage of cement hydration combined with SiO_2 to form a low alkaline C-S-H gels and tobermorite. In addition,

Table 2. Physical properties of OPC

Standard consistency/%	Fineness /%	Loss /%	Setting time/min		Stability	Flexural strength /MPa		Compressive strength/ MPa	
			Initial	Finaly		3 d	28 d	3 d	28 d
26.4	2.1	2.42	90	210	qualified	5.4	8.6	20.7	52.9

Table 3. Codes of samples

Codes	source
FA	fly ash
HAC	hardened body
AC-0	heat preservation for 0 h
AC-8	heat preservation for 8 h

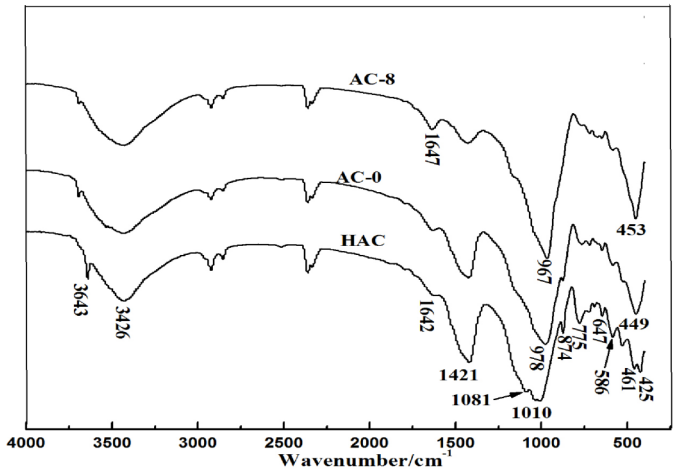

Figure 2. FT-IR spectra of samples

some AFt decomposed to form FGDG and hydrated garnet.

With the increase of the holding time, on the AC-8 curve the XRD diffraction peaks of tobermorite crystals, hydrated garnet and anhydrite were strengthened, those of AFt and $Ca(OH)_2$ disappeared, and those of the main mineral components in the original FA was significantly reduced. This indicates that after 8 hours of heat preservation, the Si-O bond and Al-O bond in the SiO_4 tetrahedral structure in the raw mineral of FA get broken under high temperature, high pressure and alkaline conditions, which promotes the dissolution rate of SiO_2 and Al_2O_3 in FA, so as to combine with more $Ca(OH)_2$ to generate corresponding hydration products (such as C-S-H gels, tobermorite, etc.). The disappeared XRD diffraction peak of AFt indicates that AFt was completely decomposed to form hydrated garnet and gypsum after 8 hours of heat preservation. During the autoclaving process, gypsum can promote the conversion of C-S-H gels to tobermorite, allowing many free cations (such as Al^{3+}, Mg^{2+}, etc.) to enter the tobermorite structure and form Al-generation (or Mg-generation) tobermorite. Also, the residual minerals (such as quartz, plagioclase, and soda feldspar) in gypsum and FA exist as aggregates in aerated concrete, which is conducive to the improvement of product strength.

In addition, by comparing the HAC, AC-0, and AC-8 curves, it's found that the XRD diffraction peaks of calcite existed in the three curves simultaneously. This is mainly due to the carbonization of the hydration products (such as C-S-H gels, tobermorite) under the influence of CO_2 in the air during the sample preparation process. However, with the extension of the holding time, the XRD diffraction peaks of calcite decreased significantly, indicating that the hydration products C-S-H gels and tobermorite crystals in aerated concrete have different carbonization resistance, and the anti-carbonization ability of tobermorite is significantly higher than that of C-S-H gels, mainly because tobermorite is a well-crystallized hydrated calcium silicate mineral, and its crystals are coarser than C-S-H gels; compared with the fine crystals of C-S-H gels, the indirect contact of the crystals is reduced, enhancing its ability to resist carbonization.

3.2. FT-IR analysis of samples

Fig. 2 shows the FT-IR spectra of HAC, AC-0 and AC-8 samples. The HAC curve shows that the absorption band with a wave number (WN) of about 3443 cm^{-1} was attributed to the stretching vibration of the hydroxyl group in $Ca(OH)_2$; the characteristic peak near the WN of 3426 cm^{-1} resulted from the stretching vibration of the water absorbed in AFt or C-S-H gels; the absorption band with the WN of about 1642 cm^{-1} was attributed to the bending vibration of hydroxyl groups in the absorbed water of the AFt or C-S-H gels; the characteristic peaks that characterize quartz were located at 1081 cm^{-1}, 775 cm^{-1} and 461 cm^{-1}, among which the characteristic peak at 1081 cm^{-1} was the asymmetric stretching vibration of Si-O, the absorption band at 775 cm^{-1} belonged to the symmetrical stretching vibration of Si-O-Si, and the characteristic peak at 461 cm^{-1} belonged to the bending vibration of Si-O; the bands with the WN around 586 cm^{-1} and 647 cm^{-1} were characterized by the bending vibration of O-Si(Al)-O, which was attributed to the vibrational bands of feldspar minerals in the original FA; the bands with a WN of about 425 cm^{-1} were characterized by vibrating bands of sodium feldspar; the broader bands with a WN of about 1000 cm^{-1} to 1050 cm^{-1} belonged to the stretching vibration of the Si-O bond caused by the hydration product C-S-H gels; the absorption bands at the WNs 1421 cm^{-1} and 874 cm^{-1} were characteristic bands of calcite, of which the absorption band at 1421 cm-^{1} belonged to the asymmetric stretching vibration of CO_3^{2-} in calcite, and the absorption band at 874 cm^{-1} was the bending vibration characteristic of CO_3^{2-} in calcite.

Compared to the HAC curve, the characteristic peaks in the AC-0 curve did not change much. After the holding time for 0h, the intensity of the absorption bands for characteristic peaks at the WNs 3643 cm^{-1}, 3426 cm^{-1}, 1421 cm^{-1}, 874 cm^{-1}, 775 cm^{-1}, 647 cm^{-1}, and 586 cm^{-1} obviously decreased, while the absorption bands at the WNs 1081 cm^{-1}, 1010 cm^{-1}, 461 cm^{-1}, and 425 cm^{-1} disappeared. This indicates that the active SiO_2 and Al_2O_3 in FA combined with $Ca(OH)_2$ to form the corresponding hydration products with the increase of temperature and pressure. The intensity of the absorption band characterizing the characteristic peaks of AFt was decreased, which indicates that some AFt has decomposed after holding for 0 hour, being consistent with the results of XRD analysis. Also, new characteristic peaks appeared on the AC-0 curve with the WNs of 978 cm^{-1} and 449 cm^{-1}, respectively; the absorption band near the WN of 978 cm^{-1} was caused by the Si-O symmetrical stretching vibration of Q^2 in the SiO_4 silicon-oxygen tetrahedron, and the absorption intensity of characteristic peak at this position was large, indicating that the vibration has strong infrared activity. The characteristic peak near the WN 449 cm^{-1} was caused by Si-O bending vibration in SiO_4 silicon-oxygen tetrahedron. The characteristic peaks with the WNs of 978 cm^{-1} and 449 cm^{-1} were all attributed to the tobermorite crystal mineral. From the XRD analysis results, the XRD diffraction peaks of quartz, plagioclase, albite and anorthite in FA were all reduced after 0 hour holding time, while the XRD diffraction peak of the tobermorite was elevated, which is in line with the analysis result of FT-IR.

In the AC-8 curve, the absorption band intensity of the characteristic peaks at the WNs of 967 cm^{-1} and 453 cm^{-1} was significantly enhanced, which indicates that after 8 hours of autoclaving, the main hydration product in the aerated concrete was tobermorite. The sharp absorption bands of characteristic peaks indicate an increase in the crystallinity of tobermorite. Meanwhile, the three characteristic curves of HAC, AC-0 and AC-8 were compared to characterize the characteristic peak of calcite, finding that its intensity of absorption band (WN at 1421 cm^{-1}) decreased gradually. From the XRD analysis results, it is mainly due to the different carbonization resistance of the hydrated tobermorite and C-S-H gels.

3.3. TG-DSC analysis of samples

Fig. 3 shows the TG-DSC analysis of HAC, AC-0, and AC-8 samples, respectively. There was a broad endothermic peak between 80 °C and 200 °C, which is mainly due to the removal of free water, adsorbed water, and weak crystalline water from hydration products such as AFt and C-S-H gels [14]. Fig. 3(a) shows that the endothermic peaks appeared on the HAC curve at 107 °C, 463 °C, 577 °C, and 762 °C. A sharp endothermic peak appeared at 107 °C, accompanied by a weight loss of 4.38%, which resulted from the dehydration of AFt according to the XRD analysis results. Through continued heating, there was a large endothermic peak at 463 °C again, mainly lying in the removal of structured water from $Ca(OH)_2$ that was formed by cement hydration or lime

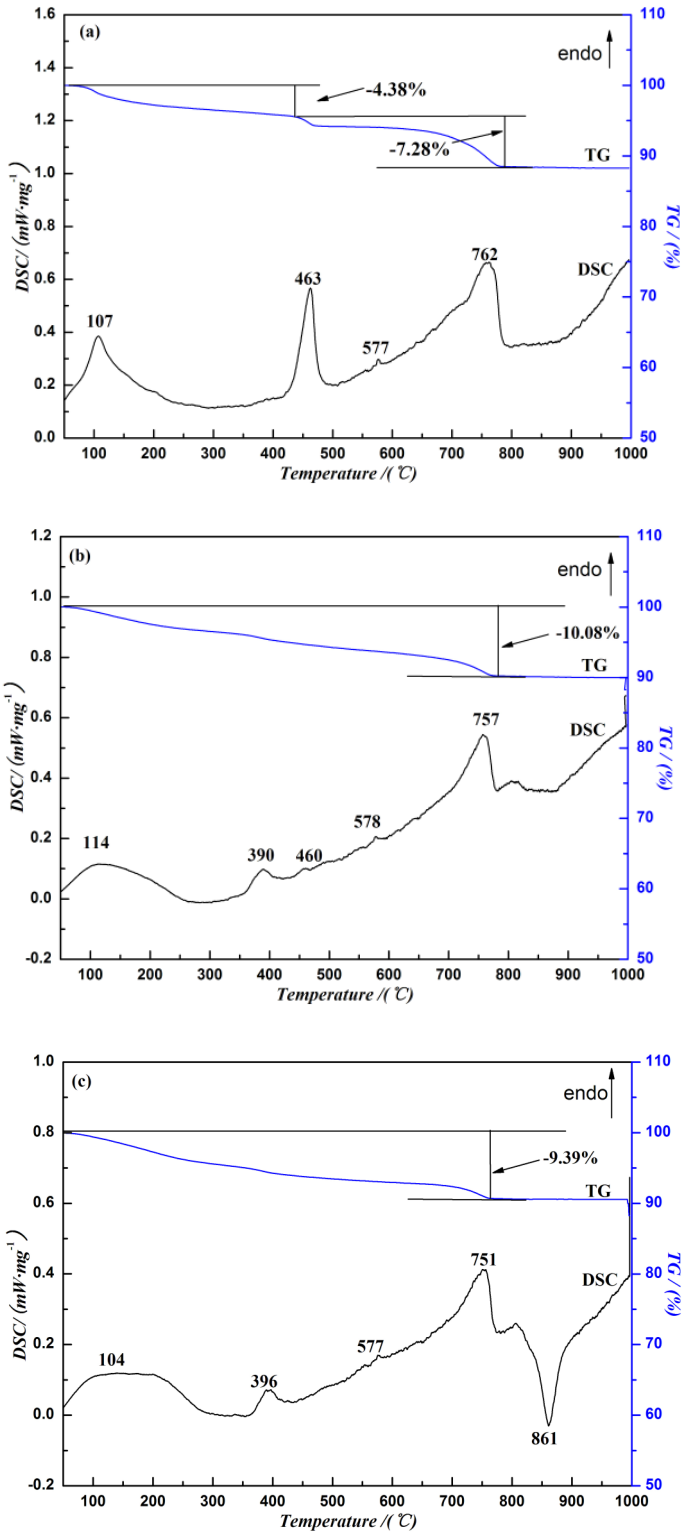

Figure 3. TG-DSC patterns of samples. (a)-HAC, (b)-AC-0, (c)-AC-8.

digestion in the HAC. The endothermic peak at 577 °C was formed by the crystal transformation of the FA, mainly from β-quartz to α-quartz [15]. At this time, no significant weight loss would occur on the TG curve. The endothermic peak at 762 °C was caused by the loss of structured water from the C-S-H gels. Also, the endothermic peak of calcite

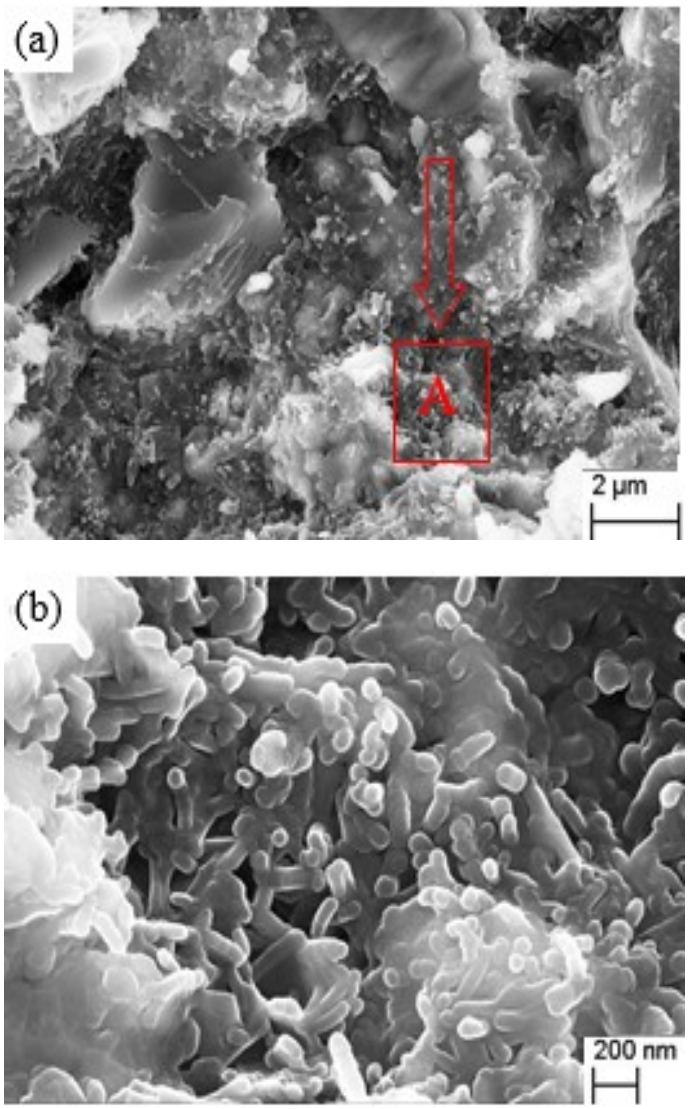

Figure 4. SEM images of sample AC-0. (a)-enlarge 10000 times, (b)-enlarge point A

decomposition was also near this temperature, thus generating a large endothermic peak.

In Fig. 3(b), the endothermic peak around 114 °C was due to dehydration of AFt; between 360 °C and 400 °C, the gypsum phases were transformed into each other; the endothermic peak that appeared at about 460 °C was formed by the dehydration of Ca $(OH)_2$, but its intensity was relatively lower compared with Fig. 3(a). This is because after autoclaving for 0 hour, $Ca(OH)_2$ in the system combined with the active components SiO_2 and Al_2O_3 in FA to form the corresponding hydration products, and then consumed, in line with the XRD and FT-IR analysis results. The absorption peak at 757 °C was the same as that in Fig. 3(a), which is caused by the complete dehydration of AFt to an anhydrous mineral. The endothermic peak at 578 °C was formed by crystal transformation of the FA.

Klimesch et al. [16] deeply analysed the hydration products of the $CaO-Al_2O_3-SiO_2-H_2O$ system by TG-DSC analysis. The results showed that the C-S-H gels can dehydrate to form franklinite at between 840 °C and 900 °C; the higher the dehydration temperature, the more Al^{3+} enters the C-S-H gels structure so that the exothermic peak formed in this

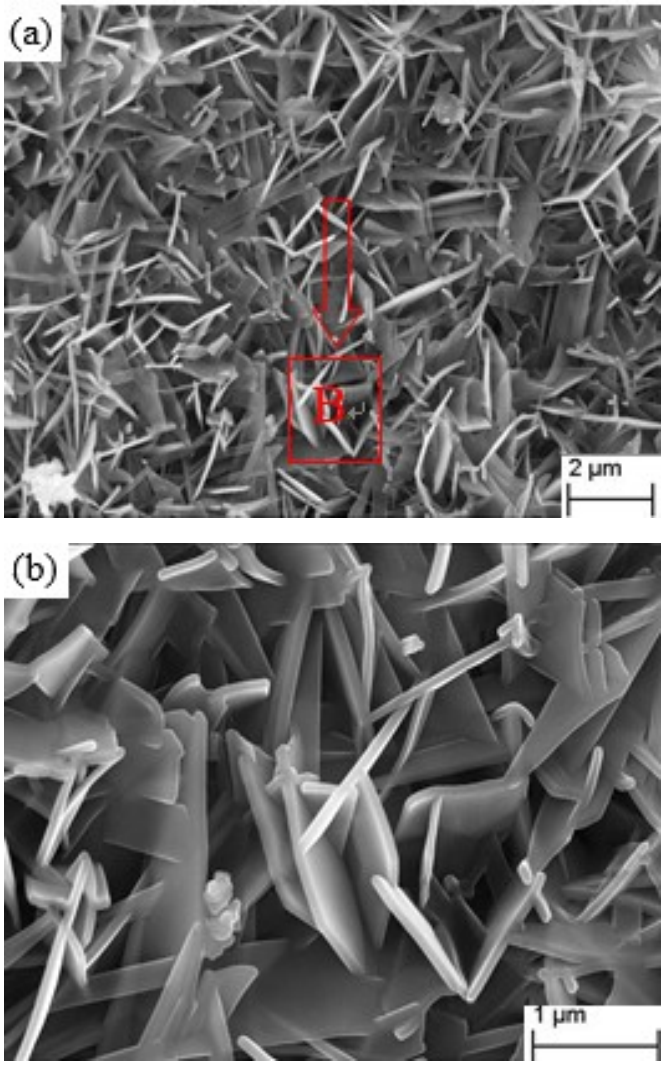

Figure 5. SEM images of sample AC-8, (a)-enlarge 10000 times, (b)-enlarge point B.

interval is attributed to Al-generation tobermorite crystal. Combined with the analysis results of XRD and FT-IR in this study, it's found that in the sample AC-8, the main hydration product of aerated concrete was tobermorite. Therefore, the high exothermic peak at 861 ºC in Fig. 3(c) was due to the crystalline transition of the tobermorite crystal. In addition, the endothermic peak at 751 ºC was formed by the decomposition of calcium carbonate, and the endothermic peak at 575 ºC was generated when the remaining quartz particles in the sample underwent crystal transformation. Besides, no endothermic peak of $Ca(OH)_2$ dehydration was not found in Fig. 3(c), which indicates that after 8 hours of autoclaving, all $Ca(OH)_2$ participated in the reaction, in line with the results of XRD and FT-IR analysis.

3.4. SEM analysis of samples

Fig. 4 and Fig. 5 show the SEM images of AC-0 and AC-8 samples, respectively. It can be seen from Fig. 4(a) that after 0 hour holding time, the hydration products in AAC were mainly C-S-H gels and AFt crystals, and the raw mineral components in the FA that did not participate in the reaction were used as aggregate, being intertwined with the hydration product. It can be seen from Fig. 4(b) that the AFt crystals in the hydration product were relatively coarse in shape and large in number, with the length between 0.1~0.3 μm. At this time, no dense network structure was formed between the hydration products, and no hydration products of tobermorite were found.

It can also be seen from Fig. 5 that in the samples AC-8, the main hydration products of the AAC were slab-shaped tobermorite crystals and lamellar C-S-H gels, and the raw mineral components not participating in the reaction was covered by the hydration products. Compared with Fig. 4, the crystallinity of the hydration products is greatly improved, and the hydration products are intertwined into a network structure. This is mainly because the active components SiO_2 and Al_2O_3 in FA were combined with $Ca(OH)_2$ in the system to form corresponding hydration products with the extension of the holding time; as the dissolution of SiO_2 and Al_2O_3 increases, the initially formed C-S-H gels with high basicity also further combined them to form C-S-H gels with low basicity and tobermorite crystals.

3.5. AAC Mechanism analysis under the autoclaved curing conditions

The reaction mechanism of AAC (cement-lime-FA AAC) is like other types of aerated concrete. The main source of its strength is also the hydration products during autoclaved curing. They mainly differ in that the siliceous material FA has different properties from silica sand and tailings, so that the hydration reaction and reaction products of the AAC also vary during autoclaving.

Under normal pressure, the hydration products of the AAC mainly come from the cement. The hydration reaction of the cement with water shall produce C-S-H gels, calcium aluminate hydrate crystals and Ca $(OH)_2$. Meanwhile, the digestion reaction between lime and water generates Ca $(OH)_2$, and releases a large amount of heat, which plays a positive role in promoting the hydration of the cement. The generated Ca $(OH)_2$ can ensure the alkalinity of the AAC slurry, which is beneficial to the dissolution of SiO_2 and Al_2O_3 active components in a small amount of ultrafine FA particles. The dissolved SiO_2 and Al_2O_3 active components combine with Ca $(OH)_2$ to form corresponding hydration products, such as C-S-H gels and calcium aluminate hydrate crystals. In the presence of gypsum, the formed calcium aluminate hydrate crystals are combined with gypsum to form the trisulfide calcium sulphoaluminate hydrate, namely AFt. Therefore, under normal pressure conditions, the main hydration products of the AAC are C-S-H gels and AFt crystals, while the solubility of SiO_2 and Al_2O_3 is extremely low, the amount of $Ca(OH)_2$ consumed is limited, and a large amount of $Ca(OH)_2$ remains in the aerated concrete body.

Under the conditions of autoclaved curing, with the increase of system temperature and pressure, AFt crystals will decompose to form hydrated garnet and gypsum, and the dissolution amount of active component SiO_2 in FA will increase. The presence of gypsum can promote the reaction of the active components SiO_2 and $Ca(OH)_2$ to form more C-S-H gels, and enhance the transformation of C-S-H gelss into tobermorite crystals to increase the crystallinity of hydration products in aerated concrete, thereby increasing the strength of aerated concrete. Therefore, after autoclaving, the main hydration products in FA aerated concrete are tobermorite crystals and C-S-H gels. The remaining mineral components in the gypsum and FA formed during the reaction exist as aggregates, which has a beneficial effect on improving the strength of the aerated concrete.

Based on the above analysis, the conversion process of hydration products in the AAC follows the basic steps below:

$$C+S+H \rightarrow C_2SH(A) \text{ or } C_2SH_2 \rightarrow C_5S_4H_n \rightarrow C_4S_5H_n \rightarrow C_4S_5H_5 \quad (1)$$

The reaction formula between the active components in FA and the remaining Ca $(OH)_2$ is as follows:

$$mCa(OH)_2+SiO_2+pH_2O\rightarrow mCaO\cdot SiO_2\cdot qH_2O \quad (2)$$

$$nCa(OH)_2+Al_2O_3+pH_2O\rightarrow nCaO\cdot Al_2O_3\cdot qH_2O \quad (3)$$

4. CONCLUSIONS

(1) Under normal pressure conditions, the main hydration products in the product were AFt and C-S-H gels with poor crystallinity, and the XRD diffraction peaks of the mineral components in FA were reduced. This indicates that under normal temperature and pressure, the FA has limited ability to participate in the reaction, and only a small number of active components participate in the reaction.

(2) Under the conditions of autoclaving and hot alkali excitation, the solubility of the active components SiO_2 and Al_2O_3 in FA increased, and the reaction ability with Ca $(OH)_2$ was enhanced, to form a C-S-H gels with high crystallinity; also, most of the mineral components in FA were decomposed, and some even disappeared, which was mainly reflected in the decrease or disappearance of the XRD diffraction peak intensity.

(3) After autoclaving for 8 hours, the hydration products in the product were tobermorite and low-basicity C-S-H gels, which are completely different from the hydration products of the HAC. A small amount of residual quartz, plagioclase and gypsum exist as aggregates, which is beneficial to the development of product strength.

(4) According to the results of the XRD, FT-IR, TG-DSC analysis, it can be seen that FA is an inert industrial waste slag under normal temperature and pressure, while it can show good activity under high temperature and pressure and alkaline excitation, and its ability of the active components SiO_2 and Al_2O_3 to participate in chemical reactions is enhanced, which plays a positive role in improving the crystallinity of the hydration products.

5. ACKNOWLEDGMENTS

The authors gratefully acknowledge financial support from China Postdoctoral Science Foundation (2016M602082), supported by Natural Science Foundation of Hebei Province (E2018402119, E2016402079), supported by Natural Science Foundation of Shaanxi Province (2019JLM-49), supported by Shaanxi Science and Technology Benefit People Project (2018ZY-HM-01), supported by Science and Technology Research Project of Higher Education Universities in Hebei Province (ZD2016014, QN2016115), supported by Comprehensive Utilization of Tailing Resources Key Laboratory of Shaanxi Province (2017SKY-WK008), supported by Jiangxi Postdoctoral Daily Fund Project (2016RC30), supported by Jiangxi Postdoctoral Research Project (2017KY19), supported by State Key Laboratory of Solid Waste Reuse for Building Materials (SWR-2019-008).

REFERENCES

[1] China association of circular economy. 2017-2018 report on comprehensive utilization and development of bulk industrial solid waste. Beijing: China Light Industry Press, 2018.

[2] Yang Y Z, Deng H W, Gao X J, Zhang A L., Materials Science and Technology, 17(2), 239 (2009).

[3] Zhang X F, Ni W, Wang Wei, Wu J Y., Materials Reports, 23(6), 93 (2009).

[4] Huang C H, Lin S K, Chang C S, Chen H J., Construction Building and Materials, 46(5), 71 (2013).

[5] Deschner F, Winnefeld F, Lothenbach B., Cement and Concrete Research, 42(10), 1389 (2012).

[6] Shakir A A, Naganathan S, Mustapha K N., Construction Building and Materials, 41(4), 131 (2013).

[7] Zeng Q, Li K F, Fen-chong T, Dangla P., Cement and Concrete Research, 42(1), 194 (2012).

[8] Wu X M, Fan Y M., Journal of South China University of Technology (Natural Science Edition), 31(8), 57 (2003).

[9] Cui K H, Ma B G, Yi H Y., Journal of the Chinese Ceramic Society, 20(2), 123 (1992).

[10]Qian X Q, Zheng L., Journal of the Chinese Ceramic Society, 19(6), 495 (1991).

[11]Saygili A, Baykal G., Energy and Buildings, 43(11), 3236 (2011).

[12]Hauser A, Eggenberger U, Mumenthaler T., Cement and Concrete Research, 29(3), 297 (1999).

[13]Kurama H, Topcu I B, Karakurt C., Journal of Materials Processing Technology, 209(2), 767 (2009).

[14]Singh M, Grag M., Cement and Concrete Research, 1995, 25(2), 332 (1995).

[15]Li M D, Qing Y., Materials Reports, 79 (1996).

[16]Klimesch D S, Ray A., Thermochemica Acta, 334(1), 115 (1999).